

The Unitary Fermi Gas in a Harmonic Trap and its Static Response

Michael McNeil Forbes

*Institute for Nuclear Theory, University of Washington, Seattle, Washington 98195-1550 USA and
Department of Physics, University of Washington, Seattle, Washington 98195-1560 USA*

(Dated: Monday 16th August, 2021)

We use harmonically trapped systems to find the leading gradient corrections of the superfluid local density approximation (SLDA) – a density functional theory (DFT) describing the unitary Fermi gas (UFG). We find the leading order correction to be negative, and predict the q^2 coefficient of the long-range static response $c_\chi = 1.5(3)$ – a factor of two smaller than predicted by mean-field theory – thereby establishing a new and experimentally measurably universal constant.

PACS numbers: 67.85.-d, 71.15.Mb, 31.15.E-, 03.75.Ss, 24.10.Cn, 03.75.Hh, 21.60.-n

UNIVERSALLY describing two-component Fermi systems with short-range interactions of infinite scattering length $a_s \rightarrow \infty$, the unitary Fermi gas (UFG) [1] not only approximates the dilute neutron matter found in neutron stars [2], but is directly realized in cold-atom systems [3], allowing experiments to benchmark many-body techniques used to study astrophysical phenomenology. Despite the simplicity of the system – the lack of length-scales, for example, implies that the equation of state $\mathcal{E}(n_+) \propto n_+^{5/3}$ – the system is strongly interacting and admits no known perturbative expansions: A quantitative description requires experiments or *ab initio* computations.

Ab initio techniques, however, can only address a few questions – direct quantum Monte Carlo (QMC) simulations, for example, can study systems with at most a few hundred particles. It is therefore imperative to benchmark computationally tractable models of macroscopic phenomena so that they can be used to answer outstanding phenomenological questions, such as the origin of glitching in neutron stars [4].

Density functional theory (DFT) is in principle exact approach, widely used in nuclear physics (see [5] for a review), and in quantum chemistry to describe normal (i.e., non-superfluid) systems. It provides a framework capable of assimilating *ab initio* and experimental results into a computationally tractable and predictive framework. In this letter, we extend one such DFT – the superfluid local density approximation (SLDA) – to describe the inhomogeneous behaviour of harmonically trapped systems. We use DFT to analyse recent experimental and theoretical results, noting discrepancies and the asymptotic behaviour toward the thermodynamic limit, and establish the leading order gradient corrections to the SLDA which we find to be negative. The SLDA then uniquely predicts the low-energy static response of the UFG to quadratic order, which is crucial for a proper low-energy description of the UFG: this therefore makes significant progress towards a predictive framework for studying superfluid phenomenology.

At low-energies, the UFG can be characterized by a superfluid effective field theory (EFT) describing phonon

dynamics [6]. The EFT admits a controlled power-counting scheme: The leading order (LO) contains a single dimensionless parameter – the Bertsch parameter [7] ξ which characterizes the equation of state $\mathcal{E}(n) = \xi \mathcal{E}_{FG}(n_+)$ where $\mathcal{E}_{FG} = 3/5 n_+ E_F$ is the energy density of a free Fermi gas with the same total density $n_+ = k_F^3/(3\pi^2)$, and $E_F = \hbar^2 k_F^2/2m$ is the Fermi energy. At next-to-leading order (NLO), two additional dimensionless coefficients [6, 8] appear which characterize the static and dynamic low-frequency and low-momentum response. We shall address only the value of the static response χ_q as defined by adding small external potential $\delta V_q(x) = \delta \cos(qx)$ to a homogeneous system:

$$\delta n_+(x) = \chi_q \delta V_q(x) + \mathcal{O}(\delta^2). \quad (1)$$

To NLO in the superfluid EFT, the response is

$$\chi(q) = \frac{-mk_F}{\hbar^2 \pi^2 \xi} \left[1 - \frac{c_\chi}{12\xi} \frac{q^2}{k_F^2} + \mathcal{O}(q^4 \ln q) \right] \quad (2)$$

where c_χ is a universal dimensionless constant [9]. This normalization for c_χ is numerically close to unity ($c_\chi = 1$ for non-interacting fermions), appears simply in the energy of trapped fermions (see Eq. (6)), and is independent of the ξ and pairing parameters in the SLDA. The other universal constant c_ω describes low-energy dynamical properties, and enters through the phonon dispersion relation [10] $\omega_q/(qc_s) = 1 + c_\omega q^2/(24\xi k_F^2) + \mathcal{O}(q^4 \ln q)$ where $c_s = \hbar k_F \sqrt{\xi/3}/m$ is the speed of sound.

While many techniques have been employed to calculate the Bertsch parameter $\xi \approx 0.37$ (see [11] for a survey), NLO coefficients have only been considered in a few cases: The ϵ -expansion [12] (expanding in spatial dimension: $\epsilon = 4 - d$) gives $c_\chi \approx 8/5 + \mathcal{O}(\epsilon^2)$ and $c_\omega \approx c_\omega + \mathcal{O}(\epsilon^2)$ [13], while Bogoliubov-de Gennes (bdG) mean-field theory [8] finds $c_\chi = 7/3$ and $c_\omega = 0.7539$.

The EFT breaks down for small systems and near the boundary of clouds, so to connect with finite-size QMC calculations, we use DFT. The Hohenberg-Kohn theorem [14] asserts the existence of a universal functional of the density alone whose minimum describes the ground state of the UFG. The exact form of this functional is

non-local and unknown, but a local formulation – an extended Thomas-Fermi (ETF) functional [12, 15–18] – describes well some energetic and dynamical aspects of the UFG. It fails, however, to properly describe finite-size effects in homogeneous systems [19, 20].

To describe these properties we use the Kohn-Sham formulation [21] which includes an auxiliary kinetic density τ_+ . While this is formally equivalent to the Hohenberg-Kohn formulation, the addition of a kinetic density allows a local formulation to describe finite-size features of the system. In particular, the finite-size properties of non-interacting systems are exactly reproduced. Interacting versions have been considered [22, 23], but one finds that the finite-size effects are not properly suppressed [19, 20]. The suppression can be realized by include an additional auxiliary anomalous density, ν , representing the pairing field [19, 20, 24], resulting in the SLDA:

$$\mathcal{E}_{\text{SLDA}} = \frac{\hbar^2}{m} \left(\frac{\alpha}{2} \tau_+ + g \nu^\dagger \nu \right) + \beta \mathcal{E}_{\text{FG}}(n_+) + \frac{\hbar^2 \delta \lambda}{8m} \frac{(\vec{\nabla} n_+)^2}{n_+},$$

$$g^{-1} = \frac{n_+^{1/3}}{\gamma} - \frac{k_c}{2\pi\alpha} \quad (3)$$

Here α is the inverse effective mass, β is the self-energy, γ controls the pairing, and $\delta \lambda$ characterizes the leading order gradient term (known as a Weizsäcker correction). The unitary limit is realized when we take the wave-vector cutoff $k_c \rightarrow \infty$ to infinity (see Ref. [24] for details). In homogeneous systems, the gradient corrections vanish, and one can use the equations in the thermodynamic limit to replace the parameters β and γ by the more physically relevant quantities ξ_S and $\eta = \Delta/E_F$, where Δ is the pairing gap (see the appendix of [20] for details). When applied to inhomogeneous systems, however, one must hold the parameters β and γ fixed to define the functional.

This form (3) subsumes earlier DFTs. In particular, the well-studied BdG mean-field equations are reproduced with unit effective mass $\alpha = 1$, $\gamma^{-1} = 0$, no Hartree term $\beta = 0$, and no gradient corrections $\delta \lambda = 0$. The Kohn-Sham form discussed in [22, 23] neglects the $\nu = 0$, while the ETF form [12, 15] is reproduced if one neglects both the anomalous density ν and the kinetic density τ_+ . As discussed in [19], none of these restricted forms can even qualitatively characterize the finite-size effects, but we still consider the ETF functional as it is much easier to solve numerically while retaining the asymptotic properties of trapped systems:

$$\mathcal{E}_{\text{ETF}} = \xi \mathcal{E}_{\text{FG}}(n_+) + \frac{\hbar^2(1/4 + \delta \lambda)}{8m} \frac{(\vec{\nabla} n_+)^2}{n_+}. \quad (4)$$

The leading gradient term here derives from a semi-classical expansion of the kinetic energy [25] with an additional Weizsäcker correction $\delta \lambda$. Superfluid hydrodynamic phenomenology [17] and vortex dynamics (appendix E) suggest that $\delta \lambda = 0$. The resulting

ETF is completely determined by the value of ξ . A simple calculation [18] shows that the ETF model has $c_\chi = c_\omega = 9/4 + 9\delta \lambda = 9/4$.

The SLDA was originally constrained by QMC calculations of the continuum state, and validated with QMC calculations in a harmonic trap [26, 27]. These validations, however, provided only a weak test of the SLDA form. In particular, the symmetric thermodynamic limit does not provide enough information to constrain the effective mass, and the original variational trap results were not sufficiently accurate to exhibit the appropriate scaling in the thermodynamic limit [19, 20].

Recently, experimental and *ab initio* QMC results for homogeneous matter in the continuum and in periodic boxes were used to more rigorously test the form of the SLDA [20]: the best fit to current unbiased results is consistent with $\xi = 0.3742(5)$, $\alpha = 1.104(8)$, and $\eta = 0.651(9)$. Here we estimate the leading order gradient correction $\delta \lambda$ by reconsidering the energies of trapped systems.

The static response in the thermodynamic limit can be calculated using the same techniques as in the BdG [8] and one finds [28]

$$c_\chi = \frac{7}{3}\alpha + 9\delta \lambda, \quad (5)$$

which is independent of ξ and η . This demonstrates how the effective mass and gradient corrections play a similar role, as pointed out in [29, 30].

From the NLO superfluid EFT [6, 8], one finds the energy of the UFG in an isotropic harmonic trap with trapping frequency ω to depend on the coefficients ξ and c_χ :

$$\frac{E}{\hbar\omega} = \frac{\sqrt{\xi}}{4} (3N_+)^{4/3} \left[1 - \frac{c_\chi}{2\xi(3N_+)^{2/3}} + \mathcal{O}\left(\frac{1}{N_+^{7/9}}\right) \right].$$

This form naturally suggests the abscissa $x = (3N_+)^{-2/3}$ so that the asymptotic behavior of E is linear: we prefer to use the square of the energy E^2 ,

$$y = \frac{16E^2}{\hbar^2\omega^2(3N_+)^{8/3}} = \xi + c_\chi x + \mathcal{O}(x^{7/6}), \quad (6)$$

as ξ appears on the intercept, and c_χ appears directly. It is interesting that, in the non-interacting system, shell-effects appear at the same linear order x , leading to a fundamental uncertainty in the coefficient $\frac{2}{3} \leq c_\chi \lesssim 1.7$. Pairing suppresses these shell effects, yielding a well-defined asymptotic slope c_χ , which can also be determined from the semi-classical approximation (see appendix B).

In Fig. 1 we display QMC results for trapped unitary systems. The dotted lines guide the eye through several variational bounds obtained using fixed-node QMC (FNQMC) calculations. In these methods, one avoids any sign problem by sampling a restricted set of wavefunctions with the same nodal structure as an initial reference

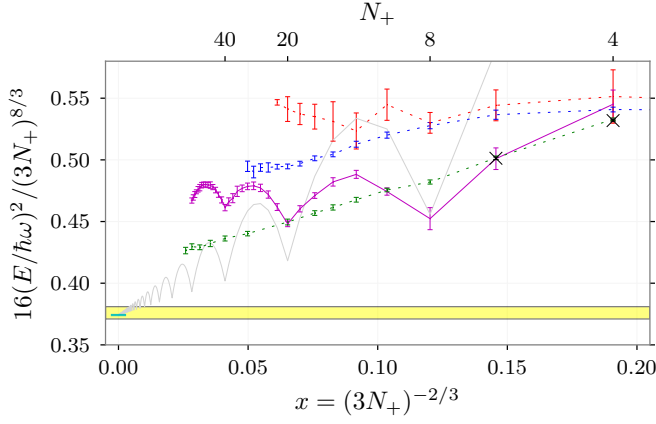


Figure 1. (color online) Various QMC and experimental results for trapped systems (with lines to guide the eye). The results with dotted lines are from FNQMC calculations that provide only upper bounds due to the nodal constraint. From top to bottom these results are from [26] (blue), [27] (red), and [20] (green). The (magenta) points with solid lines are from a lattice calculation [31] that is in principle unbiased. The large (black) crosses for $N_+ \in \{4, 6\}$ are from [32]. The solid light (grey) curve shows the shell structure for free fermions in the trap (the curve has been shifted down from 1 to facilitate comparison). Finally, we include the latest experimental value for $\xi = 0.376(5)$ from [33] as a (yellow) band and the best fit value of $\xi = 0.3742(5)$ to all homogeneous *ab initio* QMC results from [20] at $x = 0$. Coordinates have been scaled as in (6) to demonstrate the scaling. The corresponding particle numbers N_+ are listed along the top axis, and emphasize the closed shells which occur for $N_+ \in \{2, 8, 20, 40, 70\}$. (Note that all methods agree for the point $N_+ = 2$ (not shown) which admits an analytic solution.)

ansatz. By improving the ansatz and varying the parameters, these bounds have come down over time, and the lowest (green) curve [20] represents the best bound to date. Note that this is the only set of results that demonstrates the expected linear scaling (6) predicted by the effective theory. We suspect that numerical issues or the nature of the ansatz in the other cases introduced spurious lengths scales that violate this scaling (see [20] for further discussion.)

The solid (magenta) line guides the eye through calculations based on lattice techniques [31]. In principle, these are unbiased *ab initio* results, but it is somewhat troubling that most lie significantly above the variational bounds. They also display large shell effects that are virtually absent in the FNQMC results. For comparison, we have included the energies of free particles shown in Fig. 4 as a light (grey) curve, shifted down from 1 to facilitate comparison. As we shall see, although the non-interacting SLDA reproduces these shell-effects, the interacting SLDA exhibits a marked lack of shell effects, consistent with the FNQMC. The lattice results thus seem qualitatively inconsistent with the others.

A third variational technique [32] based on a corre-

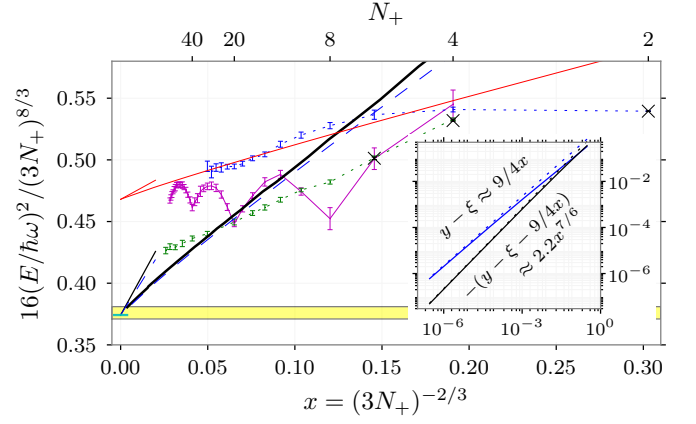


Figure 2. (color online) DFT models compared with data from Fig. 1. The thick solid (black) curve is the SLDA with parameters $\xi = 0.3742(5)$, $\alpha = 1.104(8)$, and $\eta = 0.651(9)$ but no gradient corrections $\delta\lambda = 0$. The thin dashed (blue) curve is the ETF with the same $\xi = 0.3724$ and $\delta\lambda = 0$. For comparison, the upper thin solid (red) curve corresponds to the best fit ETF model ($\xi = 0.468$, $\delta\lambda = -0.164$) described in [15] to the FNQMC result [27]. The linear asymptotic forms $y = \xi + c_\chi x$ with $c_\chi = 7\alpha/3 \approx 2.58$ (SLDA) and $c_\chi = 2.25$ (ETF) are shown as short thin lines extending from $x = 0$. The inset is a log-log plot of the deviation the ETF model makes from the asymptotic form $y = \xi + 9/4x + \alpha x^{7/6} + \dots$ where $\alpha \approx -2.2$: the solid curves are the deviations $(y - \xi)$ above (blue) and $-(y - \xi - 9/4x)$ below (black)) while the dotted lines are the expected order ($9/4x$ above and $\alpha x^{7/6}$ below).

lated Gaussian approach provides very tight bounds, but is limited to small systems. These are shown as (black) crosses for $N_+ \in \{2, 4, 6\}$. Unfortunately, at these three points, all methods agree, and significant discrepancies between the lattice and FNQMC results only appear at larger N_+ .

Finally, we include the latest experimental results as a (yellow) band [33] and the best fit value of $\xi = 0.3742(5)$ to all homogeneous *ab initio* QMC results from [20] at $x = 0$. According to the scaling (6), the results should approach this point.

In figure 2 we overlay the DFT results for the trapped systems. The best fit SLDA without gradient corrections (solid) and the ETF with the same $\xi = 0.3742$ and $\delta\lambda = 0$ (dashed) have almost exactly the same structure, demonstrating the ability of the kinetic term in the SLDA to model the gradient effects of the ETF. While the DFT results appear to approach a linear asymptotic form, the actual slope c_χ determined from the static response is only realized for extremely large N_+ . This is expected due to the very slight suppression of higher order terms $\sim x^{7/6}$: to suppress these corrections by an order of magnitude requires $0.1 \approx x^{1/6}$ which implies that $N_+ \gtrsim 10^8$. Thus, there is virtually no hope of directly extracting the value of c_χ from the QMC simulations presented in Fig. 1 without using a model to extrapolate to large N_+ . Both DFT models ultimately exhibit this behaviour as we

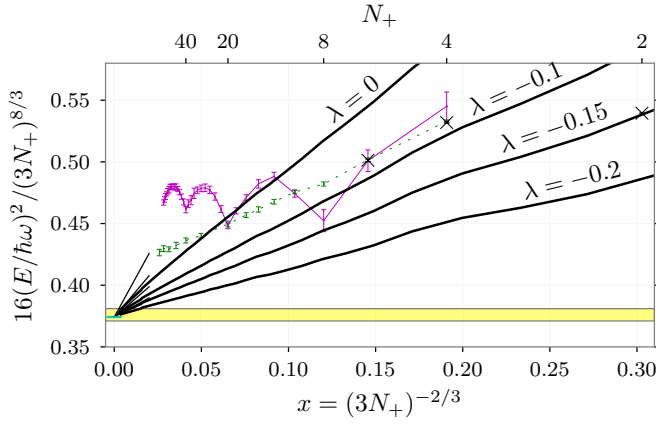


Figure 3. (color online) SLDA model as in Fig. 2 with various values of the gradient corrections λ added perturbatively.

demonstrate with the ETF in the inset.

Note that the SLDA predicts higher energies for systems with small particle numbers – especially the $N_+ \in \{2, 4, 6\}$ systems where all *ab-initio* methods agree. To correct for this, the leading gradient correction needs to be negative $\lambda < 0$. We explore these effects in Fig. 3 by perturbatively including the gradient for various values of λ . (Note: these corrections are less than 15% for all systems as shown in Fig. 5. The remaining corrections from a fully self-consistent solution will not significantly alter these results.) One could also increase the effective mass, but to match even the modest correction of $\lambda \lesssim -0.1$ requires $m_{\text{eff}} \gtrsim 1.4m$ which spoils the description of homogeneous systems [19, 20] and quasi-particle dispersions [34]. Higher order gradient corrections might help, however, there are several different gradient corrections – each requiring additional coefficients – and insufficient *ab-initio* results to constrain these. These neglected terms will not affect the coefficient c_χ . Finally, there is the possibility that the functional could be generalized as discussed in [19], but the success of the three-parameter SLDA [20] suggests that corrections along this line would be small.

We note that a negative gradient correction is somewhat surprising since a naïve expansion of an attractive non-local interaction $-V(x-y)n(x)n(y)$ yields a positive gradient correction (see appendix F).

Thus, we conclude from Fig. 3 that the SLDA will require $\lambda \approx -0.12(3)$ to describe both homogeneous boxes and trapped systems. The SLDA therefore predicts

$$c_\chi \approx 1.5(3) \quad (7)$$

where the error is approximate (not to be taken as a standard deviation). This is about half the value predicted by the bdg mean-field calculation, though the effect in the static response (2), $\propto c_\chi/\xi$, is cancelled by the excessively large bdg value of $\xi = 0.5906$. Intuitively, c_χ/ξ is four times larger than in the non-interacting system,

indicating that momentum-dependent density fluctuations are suppressed by interaction, though this effect is mostly due to the reduced value of ξ .

As discussed, c_χ cannot be directly extracted from the QMC results without a model capable of extrapolating well into the thermodynamic limit. To extract c_χ more directly, one should consider systems that minimize the sensitivity to the breakdown of the EFT at the boundary of the system. To do this, consider how the density $n \equiv n(\vec{x})$ depends on a smoothly varying potential $V \equiv V(\vec{x})$:

$$n = n_{\text{TF}}(\vec{x}) \left\{ 1 - \frac{c_\chi}{64} \frac{(\vec{\nabla}V)^2 + 4(\mu - V)\nabla^2 V}{(\mu - V)^3} \frac{\hbar^2}{m} + \dots \right\},$$

$$n_{\text{TF}}(\vec{x}) = \frac{8[\mu - V]^{3/2}}{3\pi^2(2\xi)^{3/2}} \left(\frac{m}{\hbar^2} \right)^{3/2}. \quad (8)$$

This is valid to NLO in a static background with constant phase (i.e. not near a vortex). Thus, one can directly search for deviations from the Thomas-Fermi (TF) profile that are sensitive to gradients in the potential. Applying a modulation $V \propto \cos(qx)$ directly probes the static response and is feasible in QMC simulations. Optical lattices could be used similarly in experiments, however, measuring the density to sufficient accuracy is likely to be a challenge – to compensate for the numerical suppression $c_\chi/64$ while avoiding contamination from higher-order terms will require percent level accuracy. Experiments should thus probably retain traps with axial or spherical symmetry so they can benefit from averaging techniques like the inverse Abel transform to reduce noise in $n(\vec{x})$. Adding a small dimple to the core of the trap with varying widths will allow experiments to probe the response while retaining the benefits of averaging to reduce noise.

Confirming the value of c_χ will provide an important validation of the SLDA functional, and provides another benchmark for models of the UFG: To reliably predict low-energy behaviour of the UFG, a model should reproduce the LO and NLO coefficients – ξ , c_χ , and c_ω – of the superfluid EFT

ACKNOWLEDGMENTS

We thank D. Blume, A. Bulgac, R.J. Furnstahl, S. Gandolfi, A. Gezerlis, S. Reddy, R. Sharma, and D.T. Son for useful discussions. This work is supported by US Department of Energy (DOE) grant DE-FG02-00ER41132.

Appendix A: Contradictory QMC Results

As noted in Fig. 1, there are unresolved contradictions in the QMC results for larger N_+ with the lattice results [31] exceeding the FNQMC variational bounds [20]. It would be useful to have an alternative method calculate the energies for $N_+ = 8$ and $N_+ = 12$ to resolve between these:

$$\begin{aligned} \frac{E_{\text{lat}}}{\hbar\omega} &= 11.64^{+0.106}_{-0.124} & \frac{E_{\text{FNQMC}}}{\hbar\omega} &\leq 12.01(2) & (N_+ = 8) \\ \frac{E_{\text{lat}}}{\hbar\omega} &= 20.765^{+0.045}_{-0.093} & \frac{E_{\text{FNQMC}}}{\hbar\omega} &\leq 16.07(2) & (N_+ = 12) \end{aligned}$$

Appendix B: Semiclassical Expansion

The superfluid EFT is closely related to the well-studied semiclassical expansion (in \hbar) [25] for non-interacting systems, and one can derive similar expressions to those arising from the EFT. The utility of the EFT is to organize the universal coefficients for the interacting superfluid system.

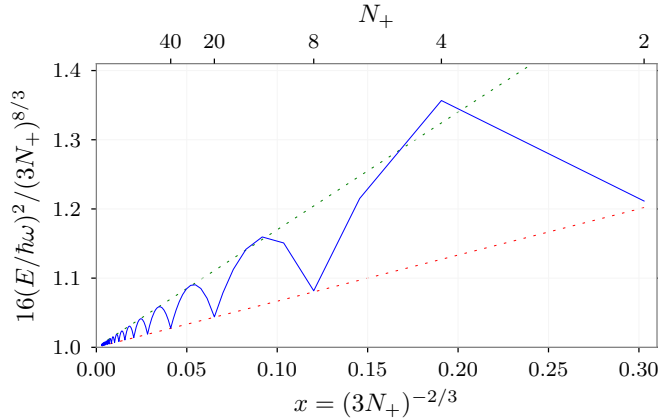


Figure 4. (color online) Shell effects in the trapped non-interacting two-component gas. The scaling is the same as in Fig. 1. The asymptotic bounds $\frac{2}{3} \leq c_\chi \lesssim 1.7$ have been drawn as dotted lines.

The shell effects for non-interacting systems is shown in Fig. 4 (this was shifted down to match ξ for comparison in Fig. 1). The semiclassical expansion systematically organizes contributions from volume effects, surface effects, periodic orbits, etc. It thus provides some insight into the breakdown of the EFT: shell for the harmonic trap, for example, effects appear at the same order as the NLO corrections. These are shown in Fig. 4 demonstrating a fundamental uncertainty in the slope $\frac{2}{3} \leq c_\chi \lesssim 1.7$. Considering the static response allows one to extract the non-interacting value of $c_\chi = 1$, which lies in this band. The fact that these corrections appear at the same order is related to nearby breakdown of the EFT formula, and the subsequent slow approach to the asymptotic scaling in the thermodynamic limit. What is non-trivial is that

pairing acts to sufficiently suppress these shell effects so that a well defined slope emerges in harmonically trapped systems. Perhaps this can be explained within the semiclassical theory, but the author is not aware of such a discussion in the literature.

Appendix C: Perturbative Gradient Corrections

In Fig. 3 we show the size of the gradient corrections E_{grad} as a percent of the total energy E for the $\delta\lambda = -0.15$ required to bring the SLDA in rough accordance with the smallest trapped systems. This demonstrates that the gradient corrections may be included perturbatively, simplifying the numerical calculations.

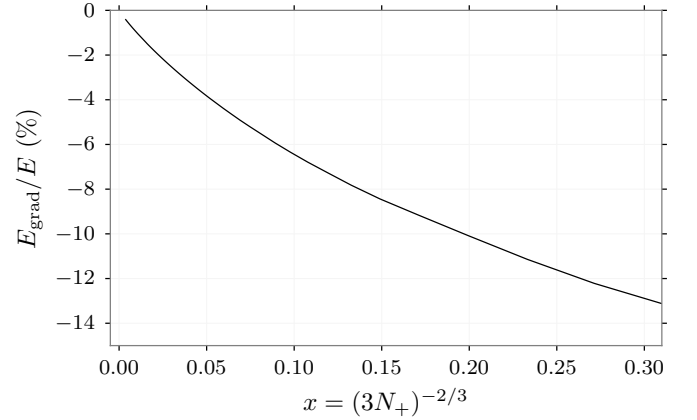


Figure 5. With E_{grad}/E (in percent) for $\delta\lambda = -0.15$, demonstrating that the correction is indeed perturbative.

In order to perform a fully self-consistent calculation of the gradient corrections, one must modify the single-particle self-energy to include a term

$$U_{\text{grad}} = -\frac{\hbar^2 \delta\lambda}{8m} \vec{\nabla} \cdot \left(\frac{\vec{\nabla} n_+}{n_+} \right) = \frac{\hbar^2 \delta\lambda}{8m} \left(4 \frac{\nabla^2 \sqrt{n_+}}{\sqrt{n_+}} - \frac{\nabla^2 n_+}{n_+} \right).$$

Accurately computing the derivatives – especially in the tails of the cloud – presents a mild numerical challenge, and will only alter the energies at the percent level, and so is not required for the present analysis. This self-consistency will be important, however, if one wants to compare the density profile of the smallest trapped systems with QMC results.

Appendix D: Asymptotic Behaviour

Figure 6 is a full-sized version of the inset of Fig. 2. This shows on a log-log scale the deviation of the numerically computed $y(x)$ from the EFT model from the expected asymptotic form (6) $y = \xi + c_\chi x - 2.2x^{7/6} + \dots$. (We do not claim anything universal about the coefficient 2.2

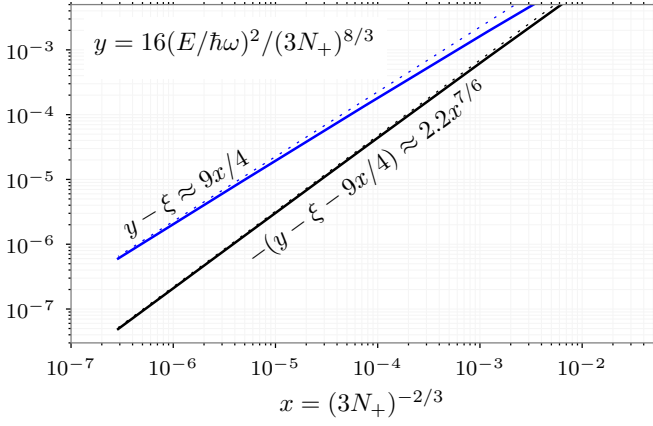


Figure 6. (color online) Asymptotic behaviour of the ETF model with $\xi = 0.3742$ and $\delta\lambda = 0$: $y = \xi + 9x/4 + \alpha x^{7/6} + \dots$ where $\alpha \approx -2.2$. We plot the deviations $y - \xi$ (upper solid blue curve) and $-(y - \xi - 9x/4)$ (lower solid black curve) along with the next terms $9x/4$ (upper dotted blue line) and $2.2x^{7/6}$ (lower dotted black line) to demonstrate the asymptotic powers.

here. It was simply obtained numerically by fitting the asymptotic form: likely, a more careful analysis of the SLDA results will yield a different value.) This confirms that the ETF does approach the asymptotic form, but only for $N_+ \sim 10^8$ as expected from the proximity of the correction. We also show the same analysis for the SLDA in Fig. 7, however, since it is much more expensive numerically, we have not approached the $N_+ \approx 10^8$ threshold (note the different scales). Although the agreement does not seem as good, this is simply a function of the small particle numbers: a comparison with the ETF results in the same region shows similar deviations.

Appendix E: No Weisacker Term in the ETF Model

Superfluid hydrodynamic simulations with the ETF find phenomenologically that the ETF without gradient corrections works best to describe collisional dynamics in the UFG [17]. Here we also argue that they must vanish to give a sensible description of vortices. The ETF model (4) is equivalent to a modified Gross-Pitaevskii Equation (GPE) [16, 35] with a complex field Ψ describing dimers of mass $2m$ normalized such that the density $n_+ = 2|\Psi|^2$:

$$i\partial_t \Psi = \left[\frac{-\hbar^2 \nabla^2}{4m} + 2(\xi E_F(n_+) - \mu) - \delta\lambda \frac{\hbar^2 \nabla^2 |\Psi|}{m|\Psi|} \right] \Psi.$$

Consider a single stationary vortex $\Psi \propto e^{i\phi} f(r)$ embedded in a uniform gas with background chemical potential $\mu = \xi E_F(n_+^\infty) = b f^{4/3}(r = \infty)$. The phase yields a centrifugal term:

$$\left(\frac{\hbar^2}{4mr^2} - \frac{(1 + 4\delta\lambda)\hbar^2 \nabla^2}{4m} + b f^{4/3}(r) - \mu \right) f(r) = 0. \quad (\text{E1})$$

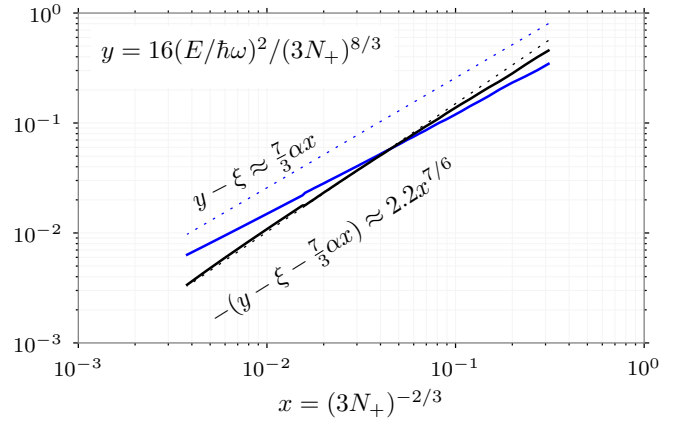


Figure 7. (color online) Asymptotic behaviour of the SLDA model with $\alpha = 1.104(8)$, $\xi = 0.3742(5)$, and $\eta = 0.651(1)$: $y = \xi + 7\alpha x/3 + \alpha x^{7/6} + \dots$ where $\alpha \approx -2.2$. We plot the deviations $y - \xi$ (upper solid blue curve) and $-(y - \xi - 7\alpha x/3)$ (lower solid black curve) along with the missing correction terms $7\alpha x/3$ (upper dotted blue line) and $2.2x^{7/6}$ (lower dotted black line) to demonstrate the asymptotic powers. Note that the scale is quite different from figure 6 owing to the additional computational complexity of the SLDA. The approach to the asymptotic form is consistent.

The Weizsäcker term modifies the effective mass in the gradient term, but does not similarly alter the centrifugal term (the first term in Eq. (E1)) since it acts only on the modulus $|\Psi|$. The vortex develops a cusp near the core: let $f(r) = ar^\alpha$ where $\alpha \approx 1$; then

$$\frac{ar^{\alpha-2}}{4m} - \frac{1 + 4\delta\lambda}{4m} a\alpha^2 r^{\alpha-2} = ba^{7/3} r^{7\alpha/3} - \mu ar^\alpha$$

The terms on the left-hand-side are divergent and must cancel, fixing $\alpha^{-2} = 1 + 2\delta\lambda$. With no Weizsäcker term $\delta\lambda = 0$, this yields the familiar $\alpha = 1$, but the presence of a Weizsäcker spoils the cancellation between the gradient and centrifugal terms, and the density profile of a vortex at the core becomes non-analytic with a cusp of a fractional power. This non-analytic cusp causes unphysical dynamical evolution of the vortex.

Appendix F: Naïve Gradient Corrections

To show that a negative gradient correction is somewhat surprising, consider expanding a local interaction in terms of the separation $\vec{r} = (\vec{x} - \vec{y})/2$ in the spirit of the density-matrix expansion (DME) [36]:

$$\begin{aligned} V(\vec{x} - \vec{y})n(\vec{x})n(\vec{y}) &\sim V(2\vec{r})n(\vec{R} + \vec{r})n(\vec{R} - \vec{r}) \\ &\sim V(2\vec{r})n^2(\vec{R}) - 2V(2\vec{r})[\vec{r} \cdot \vec{\nabla} n(\vec{R})]^2 \end{aligned}$$

Thus, a naïve expansion for an attractive potential would imply a positive gradient correction. It is apparent that this simplistic argument does not apply to the strongly interacting UFG.

-
- [1] W. Zwerger, ed., *The BCS–BEC Crossover and the Unitary Fermi Gas*, Lecture Notes in Physics, Vol. 836 (Springer-Verlag, Berlin Heidelberg, 2012).
- [2] Dilute neutron matter is also well modelled by the UFG [37] as a consequence of the unnaturally large neutron-neutron scattering length: $a_{nn} \approx -18.9(4)$ fm [38] while densities are on the order of $k_F^{-1} \sim 1$ fm. The effective s range, however, is not small: $r_{nn} \approx 2.75(11)$ fm [39] implying $k_F r_e \approx 3$. Thus, range corrections must generally be included to quantitatively describe these systems. Despite this complications, the qualitative properties of dilute neutron matter are well described by the UFG.
- [3] The scattering length of dilutely trapped alkali atoms may be tuned $|a_s| \gg k_F^{-1} \gg r_e$ such that the UFG may be directly realized in systems of cold atoms (see Refs. [1, 40] for reviews).
- [4] P. W. Anderson and N. Itoh, *Nature* **256**, 25 (1975).
- [5] J. E. Drut, R. J. Furnstahl, and L. Platter, *Prog. Part. Nucl. Phys.* **64**, 120 (2010), arXiv:0906.1463.
- [6] D. T. Son and M. B. Wingate, *Ann. Phys. (NY)* **321**, 197 (2006), arXiv:cond-mat/0509786.
- [7] “The Many-Body Challenge Problem (MBX) formulated by G. F. Bertsch in 1999,”; G. A. Baker, Jr., *Phys. Rev. C* **60**, 054311 (1999); *Recent Progress in Many-Body Theories*, Int. J. Mod. Phys. B Series on Advances in Quantum Many-Body Theory, **15**, 1314 (2001).
- [8] Mañes, L. Juan, and M. A. Valle, *Ann. Phys. (NY)* **324**, 1136 (2009), arXiv:0810.3797.
- [9] In the notations of [6], $c_x \equiv -6\pi^2(2\xi)^{3/2}(2c_1 - 9c_2)$ while in the notations of [8], $c_x \equiv -12\pi^2(2\xi)^{3/2}c_1$.
- [10] In [6], $c_\omega \equiv -6\pi^2(2\xi)^{3/2}(2c_1 + 3c_2)$ while in [8], $c_\omega \equiv -12\pi^2(2\xi)^{3/2}(c_1 - 3c_2)$.
- [11] M. G. Endres, D. B. Kaplan, J.-W. Lee, and A. N. Nicholson, “Lattice Monte Carlo calculations for unitary fermions in a finite box,” (2012), arXiv:1203.3169.
- [12] G. Rupak and T. Schaefer, *Nucl. Phys.* **A816**, 52 (2009), arXiv:0804.2678.
- [13] To compare with [12], their $c_s = c/2\xi$.
- [14] P. Hohenberg and W. Kohn, *Phys. Rev.* **136**, B864 (1964).
- [15] L. Salasnich and F. Toigo, *Phys. Rev. A* **78**, 053626 (2008), arXiv:0809.1820; *Phys. Rev. A* **82**, 059902 (2010); M. Manzoni, B.Sc. Thesis, University of Milano (2010).
- [16] L. Salasnich, F. Ancilotto, and F. Toigo, *Laser Phys. Lett.* **7**, 78 (2010), arXiv:0909.2344.
- [17] F. Ancilotto, L. Salasnich, and F. Toigo, “Shock waves in strongly interacting Fermi gas from time-dependent density functional calculations,” (2012), arXiv:1206.0568; “Dispersive effects in the unitary fermi gas,” (2012), arXiv:1210.2437.
- [18] L. Salasnich, “Contact intensity and extended hydrodynamics in the bcs-bec crossover,” (2012), arXiv:1210.3508.
- [19] M. M. Forbes, S. Gandolfi, and A. Gezerlis, *Phys. Rev. Lett.* **106**, 235303 (2011), arXiv:1011.2197.
- [20] M. M. Forbes, S. Gandolfi, and A. Gezerlis, *Phys. Rev. A* **86**, 053603 (2012), arXiv:1205.4815.
- [21] W. Kohn and L. J. Sham, *Phys. Rev.* **140**, A1133 (1965).
- [22] T. Papenbrock, *Phys. Rev. A* **72**, 041603 (2005), arXiv:cond-mat/0507183.
- [23] A. Bhattacharyya and T. Papenbrock, *Phys. Rev. A* **74**, 041602 (2006), arXiv:nucl-th/0602050.
- [24] A. Bulgac, *Phys. Rev. A* **76**, 040502 (2007), arXiv:cond-mat/0703526; A. Bulgac, M. M. Forbes, and P. Magierski, “The Unitary Fermi Gas: From Monte Carlo to Density Functionals,” Chap. 9, pp. 305 – 373, vol. 836 of [1] (2012), arXiv:1008.3933.
- [25] M. Brack and R. K. Bhaduri, *Semiclassical physics*, Frontiers in physics, Vol. 96 (Addison-Wesley, Advanced Book Program, Reading, Mass., 1997); P. Ring and P. Schuck, *The nuclear many-body problem*, 1st ed., Theoretical and Mathematical Physics Series No. 17 (Springer-Verlag, Berlin Heidelberg New York, 2004).
- [26] S.-Y. Chang and G. F. Bertsch, *Phys. Rev. A* **76**, 021603 (2007), arXiv:physics/0703190.
- [27] D. Blume, J. von Stecher, and C. H. Greene, *Phys. Rev. Lett.* **99**, 233201 (2007), arXiv:0708.2734 [cond-mat].
- [28] M. M. Forbes, Y.-L. Luo, and R. Sharma, “Static and dynamic response of the unitary fermi gas.” (in progress) (2012).
- [29] A. Bulgac, C. Lewenkopf, and V. Mickrjukov, *Phys. Rev. B* **52**, 16476 (1995), arXiv:chem-ph/9508001.
- [30] A. Bhattacharyya and R. J. Furnstahl, *Phys. Lett. B* **607**, 259 (2005), arXiv:nucl-th/0410105.
- [31] M. G. Endres, D. B. Kaplan, J.-W. Lee, and A. N. Nicholson, *Phys. Rev. A* **84**, 043644 (2011), arXiv:1106.5725.
- [32] D. Blume and K. M. Daily, *C. R. Phys.* **12**, 86 (2011), arXiv:1008.3191.
- [33] M. J. H. Ku, A. T. Sommer, L. W. Cheuk, and M. W. Zwierlein, *Science* **335**, 563 (2012), arXiv:1110.3309.
- [34] J. Carlson and S. Reddy, *Phys. Rev. Lett.* **100**, 150403 (2008), arXiv:0711.0414 [cond-mat].
- [35] M. M. Forbes and R. Sharma, “Fermion dynamics from Gross-Pitaevskii-like Equations,” in prep. (2012).
- [36] J. W. Negele and D. Vautherin, *Phys. Rev. C* **5**, 1472 (1972); *Phys. Rev. C* **11**, 1031 (1975).
- [37] A. Gezerlis and J. Carlson, *Phys. Rev. C* **77**, 032801 (2008), arXiv:0711.3006.
- [38] D. E. Gonzalez Trotter, F. S. Meneses, W. Tornow, C. R. Howell, Q. Chen, A. S. Crowell, C. D. Roper, R. L. Walter, D. Schmidt, H. Witała, W. Glöckle, H. Tang, Z. Zhou, and I. Šlaus, *Phys. Rev. C* **73**, 034001 (2006); Q. Chen, C. R. Howell, T. S. Carman, W. R. Gibbs, B. F. Gibson, A. Hussein, M. R. Kiser, G. Mertens, C. F. Moore, C. Morris, A. Obst, E. Pasyuk, C. D. Roper, F. Salinas, H. R. Setze, I. Šlaus, S. Sterbenz, W. Tornow, R. L. Walter, C. R. Whiteley, and M. Whitton, *Phys. Rev. C* **77**, 054002 (2008).
- [39] G. A. Miller, B. M. K. Nefkens, and I. Ålaus, *Phys. Rep.* **194**, 1 (1990).
- [40] M. Inguscio, W. Ketterle, and C. Salomon, eds., *Ultracold Fermi Gases*, International School of Physics “Enrico Fermi”, Vol. 164 (IOS Press, Amsterdam, 2007); S. Giorgini, L. P. Pitaevskii, and S. Stringari, *Rev. Mod. Phys.* **80**, 1215 (2008), arXiv:0706.3360.